Outer Versus Inner Halo Globular Clusters: NGC 7492 Abundances[1]

Judith G. Cohen[2] and Jorge Melendez[2]

ABSTRACT

We have carried out a detailed abundance analysis for 21 elements in a sample of four RGB stars in the outer halo globular cluster NGC 7492 (R_{GC} 25 kpc); we find [Fe/H] $= -1.82$ dex inferred from Fe I lines (-1.79 from Fe II) using high dispersion (R$=\lambda/\Delta\lambda=35{,}000$) spectra obtained with HIRES at the Keck Observatory. Most elements show no sign of star-to-star variation within our limited sample. We have, however, detected an anti-correlation between O and Na abundances similar to that seen in our previous analyses of inner halo GCs as well as in studies of relatively nearby GCs by others.

We compare the abundance ratios in NGC 7492 with those we previously determined for the much closer old halo GCs M3 and M13. After making corrections for trends of abundance ratio with metallicity characteristic of halo stars, we find that for for these three GCs for each of the elements in common we deduce identical abundance ratios with respect to Fe to within the probable measurement uncertainties. Thus, the chemical history of the outer halo as exemplified by the metal-poor outer halo globular cluster NGC 7492 is indistinguishable from that of the inner halo, exemplified by M3 and M13, at least through the epoch of formation of these old globular clusters. This applies to the neutron capture processes as well.

Subject headings: globular clusters: general — globular clusters: individual (NGC 7492) — Galaxy: halo – stars: abundances

1. Introduction

Abundance determinations of stars in Galactic globular clusters can provide valuable information about important astrophysical processes such as stellar evolution, stellar structure, Galactic chemical evolution and the formation of the Milky Way. With the advent of efficient high resolution spectrographs on 8-10m telescopes, it is now possible to reach at least the luminous RGB stars in even the most distant Galactic globular clusters (GCs). In our previous work in this area we have

---

explored the abundances for large samples of stars in the canonical relatively nearby GCs M71 (Ramírez *et al.* 2001; Ramírez & Cohen 2002), M5 (Ramírez & Cohen 2003) M3, and M13 (Cohen & Melendez 2005), as well as in Pal 12 (Cohen 2004), a cluster associated with the Sgr dwarf galaxy (Irwin 1999; Dinescu *et al.* 2000; Ibata *et al.* 2001). For the case of Pal 12, in addition to the difference in age of several Gyr, it being younger than the bulk of the Galactic GCs (Rosenberg *et al.* 1998, 1999), we found evidence for substantive differences between the chemical history of Pal 12 and that of the "normal" halo GCs of similar [Fe/H][1].

In the present work, we study the outer halo GC NGC 7492, a cluster which is not suspected (yet) of being part of any known stream or otherwise abnormal. We compare the abundance ratios deduced from high resolution, high signal-to-noise ratio for four giants in this distant outer halo GC with those from our recent analysis of a large sample of stars in the relatively nearby and well studied GCs M3 and M13, which have metallicities close to that of NGC 7492. We look for evidence in the deduced abundance ratios of some difference in the formation mechanisms or chemical history of GCs in the "normal" outer halo.

There has been no previous high dispersion study of NGC 7492. Zinn & West (1984) obtained [Fe/H] $= -1.5 \pm 0.3$ dex using their narrow band Q39 photometric system, Smith (1984) derived -1.34 ± 0.25 dex from the ΔS method applied to two RR Lyrae variables in the cluster, while moderate dispersion spectroscopy in the region of the infrared Ca triplet by Rutledge *et al.* (1997b) gave [Fe/H] $= -1.70 \pm 0.06$ dex.

2. Stellar Sample, Observations and T_{eff} Determination

Given the large distance of NGC 7492, we select the brightest possible stars on the upper RGB for observation, making no attempt to reach fainter luminosities. These stars were picked from the photometric study of this cluster by Cuffey (1961). Since this is a rather sparse cluster, these stars, which are the four brightest suspected members, lie distributed along the upper RGB, not concentrated at the RGB tip. The positions of these stars in a V, I CMD are illustrated in Figure 1 superposed on the predicted cluster isochrone from the Yi *et al.* (2001) evolutionary tracks; see Figure 10 of Buonanno *et al.* (1987) for a B, V CMD of NGC 7492. Although the cluster is distant, there are so few luminous giants that they must be observed as single stars; two of them cannot be fit into a single 7 arcsec long slit. Spectra were obtained with HIRES (Vogt *et al.* 1994) at the Keck Observatory 20-22 August 2003. The instrument configuration covered the range 4650 to 7010 Å, with small gaps between the orders at the red end. This is the "yellow" configuration described in Cohen & Melendez (2005). These data were reduced using a combination of Figaro (Shortridge

---

[1]The standard nomenclature is adopted; the abundance of element X is given by $\epsilon(X) = N(X)/N(H)$ on a scale where $N(H) = 10^{12}$ H atoms. Then [X/H] $= \log[N(X)/N(H)] - \log[N(X)/N(H)]_\odot$, and similarly for [X/Fe].

1993) scripts and the software package MAKEE [2].

The desired minimum SNR was 90 over a 4 pixel resolution element for a wavelength near the center of the HIRES detector. This is calculated strictly from the counts in the object spectrum, and excludes noise from cosmic ray hits, sky subtraction, flattening problems, etc. Since the nights were relatively dark, sky subtraction is not an issue except at the specific wavelengths corresponding to strong night sky emission lines, such as the Na D doublet. The seeing was extremely good during these nights, making the exposures shorter than normal, and enabling us to reach this goal for the stars reported here. Table 1 gives details of the HIRES exposures for each star, with the total exposure time for each object. All long integrations were broken up into separate exposures, each 1200 sec long, to optimize cosmic ray removal. The last column of the table gives the heliocentric radial velocity for each star, measured from the HIRES spectra; see Ramírez & Cohen (2003) for the details of the procedure used to determine v_r.

The radial velocity of NGC 7492 is large and negative, and the cluster abundance is low. It was easy to tell after one integration whether or not a star is a member of the cluster. Approximate measurements of v_r were made on line; all stars attempted turned out to be radial velocity members of NGC 7492. The four RGB stars have a mean v_r of -176.9 km s^{-1}, agreeing well within the errors with the early measurement of Hartwick & Sargent (1978) of a single bright cluster member, but somewhat larger than the value of -214 km s^{-1} found from moderate resolution spectra by Rutledge *et al.* (1997a). Our more accurate v_r for NGC 7492 should be used in future computations of the mass of the Galaxy which rely on the orbits of its outlying satellites. The velocity dispersion from the four members, with no correction for an instrumental contribution, is $\sigma = 1.2 \pm 1$ km s^{-1}, reflecting the low mass of this sparse cluster; the observed σ is only slightly larger than the expected instrumental uncertainties.

2.1. Stellar Parameter Determination

We follow the procedures developed in our earlier work on globular cluster stars and described in Cohen, Behr & Briley (2001) to determine the stellar parameters for the four RGB stars in NGC 7492. T_{eff} is derived by comparing reddening-corrected broad band colors with the predictions of grids of model atmospheres. We utilize here the grid of predicted broad band colors and bolometric corrections of Houdashelt, Bell & Sweigart (2000) based on the MARCS stellar atmosphere code of Gustafsson *et al.* (1975).

We normally utilize $V-I, V-J$ and $V-K$ colors to determine T_{eff}. The infrared colors were taken from 2MASS (Skrutskie *et al.* 1997; Cutri *et al.* 2003). Cuffey (1961) provided P, V photo-

---

[2]MAKEE was developed by T.A. Barlow specifically for reduction of Keck HIRES data. It is freely available on the world wide web at the Keck Observatory home page, http://www2.keck.hawaii.edu:3636/.

graphic photometry over a large field including the entire cluster of NGC 7492[3]. CCD photometry in B, V was presented by Buonanno *et al.* (1987), but their field is smaller than the cluster and the calibration of their photometry is not secure. Côté, Richer & Fahlman (1991), in the course of a study of blue stragglers in this cluster, obtained CCD B, V photometry for a large sample of stars, but the data tables were never published and have subsequently been lost (Côté, private communication, 2004).

The two published photometric studies of NGC 7492 give V mags which are inconsistent by several tenths of a mag; the differences are not just a simple offset. We therefore measured V, I for our sample stars from ANDICAM images taken for this purpose on Aug. 1, 2004 with the 1.3m telescope at CTIO operated by the SMARTS consortium; these values are given in Table 1. ANDICAM is a dual channel cammera constructed by the Ohio State University instrument group, but only the optical channel was used[4]. Our ANDICAM program requires photometric conditions, and additional standard star fields, charged to our ANDICAM allocation through NOAO, are always taken for us.

We adopt a distance for NGC 7492 of 26.2 kpc (Côté, Richer & Fahlman 1991) (as compared to 7.5 kpc for M13 and 10.4 kpc for M3), with a reddening of E(B–V) = 0.036 mag from Schlegel, Finkbeiner & Davis (1998). The relative extinction in various passbands is taken from Cohen *et al.* (1981) (see also Schlegel, Finkbeiner & Davis 1998). The adopted stellar parameters are given in Table 2.

2.2. Data Reduction and Analysis

To the maximum extent possible, the atomic data and the analysis procedures used here are identical to those we used in our recently completed analysis of a large sample of stars in M3 and M13 (Cohen & Melendez 2005). In particular, see §3 of that paper for a description of the measurement of the equivalent widths (listed for the four stars in NGC 7492 in Table 3), §4 for a discussion of the atomic parameters, §4.2 for our adopted Solar abundances (tabulated in Table 2 of our earlier paper, and repeated as Table 4 here), and §6 for a description of our abundance analysis procedures. As in our earlier work, the abundance analysis is carried out using a current version of the LTE spectral synthesis program MOOG (Sneden 1973). We employ the grid of stellar atmospheres from Kurucz (1993) without convective overshoot, when available. The template file of suitable unblended lines with their adopted atomic parameters is identical to that we used in our recently completed analysis of M3 and of M13 (Cohen & Melendez 2005).

Three of the four stars gave $v_t = 2.0$ km s^{-1} based on deriving a uniform Fe abundance as a

---

[3]Barnes (1968), who searched for variable stars in NGC 7492, defined his photometric system using Cuffey's measurements.

[4]See http://www.astronomy.ohio-state.edu/ANDICAM and http://www.astro.yale.edu/smarts.

function of W_λ for the large set of Fe I lines. The fourth star (Star R) gave 1.8 km s^{-1}; this value was also set to 2.0 km s^{-1}. Lines with $W_\lambda > 175$ mÅ were ignored, except for the Ba II lines in the coolest star in our sample in NGC 7492.

The resulting abundance ratios for the four RGB stars in NGC 7492 are given in Tables 5a to 5e. Species with only one detected line are assigned an uncertainty of 0.10 dex. Table 7 of Cohen & Melendez (2005) indicates the changes in derived abundance ratios for small changes in the adopted stellar parameters, the [Fe/H] for the adopted model atmosphere, or the set of W_λ for the lines of each species, and is appropriate for use here as well. The mean abundance and 1σ variance for the species observed in NGC 7492 are listed in Table 6.

2.3. Comments on Individual Elements

The oxygen abundance is derived from the forbidden lines at 6300 and 6363 Å. The subtraction of the night sky emission lines for the forbidden lines was reasonably straightforward given that the radial velocity of NGC 7492 is sufficiently different from 0 km s^{-1} that their W_λ can be reliably measured. The C/O ratio was assumed to be Solar. CN and Ni I contamination is negligable (see Cohen & Melendez 2005). [O/Fe] is given with respect to Fe II; abundance ratios for all other elements are given with respect to Fe I.

The deduced mean [Fe/H] of NGC 7492 value is in good agreement with that inferred by Rutledge *et al.* (1997b) from moderate dispersion spectra in the region of the infrared Ca triplet.

The Na abundance was obtained from the 5680 Å doublet for all four stars. We have, as in our previous papers, not used any non-LTE corrections for Na. Calculations by Gratton *et al.* (1999) suggest values of between 0.1 and 0.2 dex are appropriate for our sample in NGC 7492, with the coolest star having the largest value. Calculations by Takeda *et al.* (2003) suggest somewhat smaller values.

The Ba abundance of star 950 in NGC 7492 appears to be $\sim$0.2 dex larger than that of the other cluster members studied here. However, the detected lines of Ba II are all within the range where substantial HFS corrections occur. Table 7 of Cohen & Melendez (2005) shows the very high sensitivity of the deduced Ba abundances to small uncertainties in the equivalent width and microturbulence of the Ba II lines we use. On the other hand, the deduced [Y/Fe] is also somewhat high for this star, while the deduced Fe is the lowest of all the stars in our sample. Perhaps a slight adjustment of T_{eff} for this star is required. At this point, we assume this is the result of observational and modelling uncertainties and does not indicate a real spread in [Ba/Fe] within NGC 7492, but further verification of this is desirable.

The abundances of the elements with respect to Fe, [X/Fe], as a function of T_{eff} are shown in Figure 3, covering O, Na, Mg and Si, Figure 4, which includes Ca, Sc, Ti and V, Figure 5, which includes Cr, Mn, Co and Ni, Figure 6, which includes Cu, Zn, Y and Zr, and Figure 7, for Ba, La,

Nd, Eu and Dy. Note the apparent star-to-star variation in [O/Fe] and in [Na/Fe], which becomes undetectably small, if it exists at all, for the elements heavier than Na. The scatter for [Ca/Fe] and for [Ni/Fe], with 8 to 13 detected absorption lines in each star, is remarkably small, ≤ 0.03 dex over the four star sample in NGC 7492.

2.4. Abundance Spreads

To check for the presence of star-to-star variations in abundance ratios within the small sample of RGB stars in NGC 7492, we use a parameter we call the "spread ratio" (SR). The numerator of SR is the 1σ rms variance for the sample of four stars in NGC 7492 about the mean abundance for each atomic species (X) with detected absorption lines, denoted σ; the relevant values are given in the first three columns of Table 6. The denominator of SR is the total expected uncertainty, $\sigma(tot)$, which is the sum in quadrature of the known contributing terms. Included are a term corresponding to an uncertainty of 50 K in T_{eff}, the same for an uncertainty of 0.2 dex in $\log(g)$, and for an uncertainty of 0.2 km s^{-1} in v_t, and the observed uncertainty [$\sigma(obs)$], The parameter $\sigma(obs)$, which is calculated from data given in Tables 5a to 5e, is taken as the variance about the mean abundance for a given species in a given star, i.e. the 1σ rms value about the mean abundance of species X in a given star$/\sqrt{N}$, where N is the number of observed lines of species X. It includes contributions from errors in the measured W_λ, random errors (i.e. between lines of a given species) in the adopted gf values, etc. Some species, an example being Fe I with its very large value of N, have unrealistically small values of $\sigma(obs)$; we adopt a minimum of 0.05 dex for this parameter.

The ratio $\sigma/\sigma(tot)$ is an indication of whether there is any intrinsic star-to-star variation in [X/Fe]. A high value of this "spread ratio", tabulated in the fifth column of this table, suggests a high probability of intrinsic scatter for the abundance of the species X. Ideally the mean SR for those elements with no star-to-star variation should be unity; for many species the measured SR is close to that value, certainly closer here than for the sample in M3 and in M13 we studied earlier (Cohen & Melendez 2005).

Inspection of Table 6 shows that for all but two species $SR < 1.0$ for the sample of four stars in NGC 7492, indicating little sign of an intrinsic star-to-star range in abundance. O I and Na I, however, have the two largest values of SR, 1.3 and 3.0 respectively. Note that SR for Mg I is 0.5, suggesting no real star-to-star abundance variations for this element. We therefore assume that the range of abundances seen in our sample of RGB stars in NGC 7492 for Na I and O I represent real star-to-star abundance variations; while no other element shows definite evidence for such variations from this simple analysis.

2.5. Correlated Abundance Variations of the Light Elements

C, N, O, Na, Mg, and Al are known to show correlated abundance variations from star-to-star among the most luminous stars in globular clusters; see, e.g. the review of Kraft (1994). Our simple spread ratio analysis (see §2.4) shows definite star-to-star variations in abundance of both O and Na in our small sample of RGB stars in NGC 7492. Variations in Mg, if present are smaller and subtle.

It is well established that O and Na are anti-correlated among luminous giants in globular clusters, see, e.g. Kraft (1994). Furthermore, Ramírez & Cohen (2002) compiled the data from the literature, combined it with their own, and showed that the same linear relation can be used to fit the O and Na data for all globular clusters studied in detail thus far. The latest addition to the clusters studied in detail, NGC 2808, by Carretta, Bragaglia & Cacciari (2004), does so as well.

Figure 8 shows the relationship between Na and O abundances (both with respect to Fe) for our sample in NGC 7492. Also superposed is the line representing the fit for this anti-correlation determined by Sneden *et al.* (2004) for the luminous giants in M3, shifted by -0.07 dex and $+0.1$ dex in the vertical and horizontal axis as compared to the relation we found for M13 (Cohen & Melendez 2005). The first and last quartiles of the O–Na anti-correlation seen by Sneden *et al.* (2004) in their sample of luminous giants in M3 are indicated. There is a reasonably clear anti-correlation which corresponds well with that seen for luminous giants in other well studied Galactic GCs (see, e.g. the compilation of Cohen & Melendez 2005). A similar correlation is detected in the outer halo GC NGC 7006 by Kraft *et al.* (1998).

There is marginally statistically significant evidence for a correlation between [Na/Fe] and [Mg/Fe] for our small sample in NGC 7492, similar to that shown in other GCs (see, for example, figures 12 and 13 of Sneden *et al.* 2004). The larger uncertainty in our deduced [Mg/Fe] ratios makes this result quite uncertain.

3. Comparison with the Inner Halo GCs M3 and M13

We now turn to what we can learn about the chemical history of the Galaxy by comparing the abundance ratios in NGC 7492, at a galactocentric distance of 25 kpc, with those from our recent analysis of the inner halo GCs, M3 and M13 (Cohen & Melendez 2005) in M3 and M13, with R_{GC} of 12 and 9 kpc respectively. We note that the atomic parameters, the analysis procedures, and the software packages used are identical in both of these studies. Hence we should be able to detect small differences in the relative values of the abundance ratios of these three GCs.

Table 7 gives the parameter Δ[X/Fe], which is, for each species with detected lines, the mean abundance ratio [X/Fe] for NGC 7492 with the average of the same parameter for M3 and for M13 subtracted. Because of the large star-to-star differences in O/Fe seen in M3 and especially in M13, we subtract the mean [O/Fe] for stars in M13 of luminosities comparable to those we observe

in NGC 7492. Similarly, Cohen & Melendez (2005) found a luminosity dependence of [Mg/Fe] in M13, most probably due to the luminosity dependence of non-LTE corrections, which were ignored. Again in this case we subtract the mean [Mg/Fe] of stars of comparable luminosity in M13 to those observed in NGC 7492.

If we allow ±0.15 dex as a tolerable range given the potential internal and systematic errors in the analyses of these three GCs, we find that 80% of the 20 elements in common have a difference of 0.0±0.15 dex, with only Si, Cr and Co[5] outside that range. Figure 10 shows the resulting differences in [X/Fe] as a function of atomic number. The abundance ratios of [X/Fe] for Si and Co are each larger in NGC 7492 than they are in M3 and M13, while that of Cr is smaller. The largest magnitude of the set of Δ[X/Fe] occurs for Si, and is +0.23 dex.

Galactic chemical evolution produces trends in abundance ratios as a function of metallicity. The case of [Si/Fe] is illustrated in Figure 9, where metallicity is parameterized by [Fe/H]; examples for the elements Ca, Ti and Ba are given in Figures 21, 22 and 23 of Cohen & Melendez (2005). We use the same set of of high precision analyses of GCs as in Cohen & Melendez (2005), specifically NGC 6528 (Carretta *et al.* 2001), NGC 6553 (Cohen *et al.* 1999; Carretta *et al.* 2001), 47 Tuc (Carretta *et al.* 2004; James *et al.* 2004), M71 (Ramírez & Cohen 2002, 2003), M5 (Ramírez & Cohen 2003), NGC 288 (Shetrone & Keane 2000), NGC 362 (Shetrone & Keane 2000), NGC 6752 (James *et al.* 2004), M3 (Sneden *et al.* 2004; Cohen & Melendez 2005), M13 (Sneden *et al.* 2004; Cohen & Melendez 2005), NGC 6397 (Thévenin *et al.* 2001; Gratton *et al.* 2001; James *et al.* 2004) and M15 (Sneden *et al.* 1997), adding in NGC 7492 as well. To characterize the behavior of the metal-poor halo field stars, we adopt abundance ratios from recent large surveys of Gratton & Sneden (1991), McWilliam *et al.* (1995), Fulbright (2000), and by Johnson (2002). No effort has been made to homogenize these analyses, but since the field star surveys were carried out over the course of more than a decade, we have corrected for the difference in the Solar Fe abundance adopted by each.

Given that NGC 7492 has [Fe/H] 0.35 dex smaller than the mean value for M3 and M13, we have attempted to evaluate the correction to the difference caused by these global trends. We can only do this for about half of the elements studied here. This correction is given in the last column of Table 7, and is to be subtracted from the value of Δ[X/Fe] to form $\Delta(cor)$[X/Fe]. These corrections, which do not exceed 0.1 dex in magnitude, bring $\Delta(cor)$[Si/Fe], $\Delta(cor)$[Cr/Fe] and $\Delta(cor)$[Co/Fe] within the range consistent with no difference (0.0±0.15 dex), while not causing any additional elements to exceed the allowed range for equality. The corrections for Si, Cr and Co are shown on Figure 10 as well.

Thus after implementing the corrections for global chemical evolution, all the elements in common show identical abundance ratios [X/Fe] for NGC 7492 as for M3 and M13, allowing for

---

[5]We ignore Zr as there are only a few weak lines detected the HIRES spectrum of the coolest star in our sample in NGC 7492.

a ± 0.15 dex tolerance; 75% of the 20 values of $\Delta(cor)[X/Fe]$ lie within the range -0.10 to $+0.10$ dex. This suggests that the galactic chemical evolution of the outer halo at R_{GC} 25 kpc has been identical to that of the well studied inner halo GCs, at least up to the time of the formation of the old globular clusters NGC 7492, M3 and M13. In particular, our limited evidence, based on Ba, La and Eu abundance ratios, suggests the neutron capture processes, both r and s, appear to have had similar histories throughout the spatial extent of the halo for old GC stars.

4. Summary

We have carried a detailed abundance analysis for 21 elements in a sample of four RGB stars in the metal poor distant outer halo globular cluster NGC 7492 ([Fe/H] -1.80 dex). The analyzed spectra, obtained with HIRES at the Keck Observatory, are of high dispersion (R=$\lambda/\Delta\lambda$=35,000). Most elements show no sign of star-to-star variation within our limited sample. We have, however, detected an anti-correlation between O and Na abundances similar to that seen in our previous analyses of inner halo GCs as well as in studies of relatively nearby GCs by other. A correlation between Mg and Na abundance may also be present.

We have compared the abundance ratios in NGC 7492 with those we previously determined for the much closer old halo GCs M3 and M13 (Cohen & Melendez 2005), hoping that since all these analyses were carried out by the same two people within a timespan of only a few months in a completely consistent manner, with the same line lists, the same atomic parameters, the same analysis codes and procedures, etc. that small differences in the abundance ratios might be detectable. We evaluate the trends of abundance ratio with metallicity for old halo stars from our data combined with published large surveys of halo field star abundances. We then apply corrections to the abundances we derived for M3 and M13 for each species, when feasible, to extrapolate them to the 0.35 dex smaller [Fe/H] of NGC 7492. After making such corrections, all the elements in common show identical abundance ratios for NGC 7492 and for M3 and M13, allowing for a ± 0.15 dex tolerance, and 75% of them are then within the tolerance ± 0.10 dex. This suggests that the galactic chemical evolution of the outer halo at R_{GC} 25 kpc has been identical to that of the well studied much closer inner halo GCs, at least up to the time of the formation of the old globular clusters NGC 7492, M3 and M13. In particular, our limited evidence, based on Ba, La and Eu abundance ratios, suggests the neutron capture processes, both r and s, appear to have had similar histories throughout the spatial extent of the halo for old GC stars as well.

The presence of the O/Na anti-correlation in NGC 7492, with R_{GC} of 25 kpc, and the similarity of its chemical history to that of the well studied nearby GCs, provide new constraints on any model of GC formation in the Galactic halo.

REFERENCES

Barnes, S. A., 1968, AJ, 73, 579

Carretta, E., Cohen, J. G., Gratton, R. G. & Behr, B. B., 2001, AJ, 122, 1469

Carretta, E., Gratton, R., Bragaglia, A., Bonifacio, P. & Pasquini, L., 2004,A&A, 416, 925

Carretta, E., Bragaglia, A. & Cacciari, C., 2004, A&A, in press

Cohen, J. G., Frogel, J. A., Persson, S. E. & Elias, J. H., 1981, ApJ, 249, 481, 1981

Cohen, J. G., Gratton, R. G., Behr, B. B. & Carretta, E., 1999, ApJ, 523, 739

Cohen, J. G., Behr, B. B. & Briley, M. M., 2001, AJ, 122, 1420

Cohen, J. G., 2004, AJ, 127, 1545

Cohen, J. G. & Melendez, J., 2005, AJ (in press)

Cuffey, J., 1961, MNRAS, 122, 363

Cutri, R. M. *et al.*, 2003, "Explanatory Supplement to the 2MASS All-Sky Data Release, http://www.ipac.caltech.edu/2mass/releases/allsky/doc/explsup.html

Buonanno, R., Corsi, C. E., Ferraro, F. R. & Fusi Pecci, F., 1987,A&AS, 67, 327

Côté, P. C., Richer, H. R. & Fahlman, G. G., 1991, AJ, 102, 1358

Dinescu, D.I., Majewski, S.R., Girard, T.M. & Cudworth, K.M., 2000, AJ, 120, 1892

Fulbright, J. P., 2000, AJ, 120, 1841

Gratton, R. G., Carretta, E., Eriksson, K. & Gustafsson, B., 1999, A&A, 350, 955

Gratton, R. G. & Sneden, C., 1991, A&A, 241, 501

Gratton. R. G., *et al.*, 2001, A&A, 369, 87

Gustafsson, B., Bell, R.A., Eriksson, K. & Nordlund, A&A, 1975, A&A, 42, 407

Hartwick, F. D. A. & Sargent, W. L. W., 1978, ApJ, 221, 512

Houdashelt, M. L., Bell, R. A. & Sweigart, A. V., 2000, AJ, 119, 1448

Ibata, R., Lewis, G. F., Irwin, M., Totten, E. & Quinn, T., 2001, ApJ, 551, 294

Irwin, M. J., 1999, in *The Stellar Content of Local Group Galaxies*, ed. P.A.Whitelock & R.D.Cannon (San Francisco: ASP), 409

James, G. *et al.*, 2004, A&A, 414, 1071

James, G., Francois, P., Bonifacio, P. Carretta, E., Gratton, R. G. & Spite, F., 2004, A&A, in press

Johnson, J. A., 2002, ApJS, 139, 219

Kraft, R. P., 1994, PASP, 106, 553

Kraft, R. P., Sneden, C., Smith, G. H., Shetrone, M. D. & Fulbright, J., 1998, AJ, 115, 1500

Kurucz, R. L., 1993, ATLAS9 Stellar Atmosphere Programs and 2 km/s Grid, (Kurucz CD-ROM No. 13)

McWilliam, A., Preston, G. W., Sneden, C. & Searle, L., 1995, AJ, 109, 2757

Ramírez, S. V., Cohen, J. G., Buss, J., & Briley, M. M., 2001, AJ, 122, 1429

Ramírez, S. V. & Cohen, J. G., 2002, AJ, 123, 3277

Ramírez, S. V. & Cohen, J. G., 2003, AJ, 125, 224

Rosenberg, A., Saviane, I., Piotto , G. & Held, E. V., 1998, A&A, 339, 61

Rosenberg, A., Saviane, I., Pioto , G. & Aparicio, A., 1999, AJ, 118, 2306

Rutledge, G.A., Hesser, J. E., Stetson, P. B., Mateo, M., Simard, L., Bolte, M., Friel, E. D. & Copin, Y., 1997, PASP, 109, 883

Rutledge, G.A., Hesser, J. E. & Stetson, P. B., 1997b, PASP, 109, 907

Shetrone, M. & Keane, 2000, AJ, 119, 840

Schlegel, D. J., Finkbeiner, D. P. & Davis, M., 1998, ApJ, 500, 525

Shortridge, K., 1993, "The Figaro 2.4 Manual" (Epping: Anglo-Australian Obs.)

Skrutskie, M. F., Schneider, S.E., Stiening, R., Strom, S.E., Weinberg, M.D., Beichman, C., Chester, T. *et al.*, 1997, in *The Impact of Large Scale Near-IR Sky Surveys*, ed. F.Garzon *et al.* (Dordrecht: Kluwer), p. 187

Smith, H. A., 1984, ApJ, 281, 148

Sneden, C., 1973, Ph.D. thesis, Univ. of Texas

Sneden, C., Kraft, R. P., Shetrone, M. D., Smith, G. H., Langer, G. E. & Prosser, C. F., 1997, AJ, 114, 1964

Sneden, C., Kraft, R. P., Guhathakurta, P., Peterson, R. C. & Fulbright, J. P., 2004, AJ, 127, 2162

– 13 –

Takeda, Y., Zhao, G., Takada-Hidai, M., Chen, Y., Saito, Y. & Zhang, H. W., 2003, Chin.J.Astron.Astrophys., 3, 316

Thevenin, F., Carbonnel, C., de Freitas Pacheco, J. A., Idiart, T. P., Jasniewsicz, G., de Lavery, P. & Plez, B., 2001, A&A, 373, 905

Vogt, S. E. *et al.* 1994, SPIE, 2198, 362

Yi, S., Demarque, P., Kim, Y.-C. , Lee, Y.-W., Ree, C. Lejeune, Th. & Barnes, S., 2001, ApJS, 136, 417

Zinn, R. & West, M. J., 1984, ApJS, 55, 45

This preprint was prepared with the AAS LATEX macros v5.2.

Table 1.   The Sample of Stars in NGC 7492

ID[a]	Coords. (J2000)	V[b] (mag)	I[b] (mag)	Date Obs.	Exp. Time (sec)	SNR[c]	v_r (km s^{-1})
H, 231	23 08 22.32 −15 37 43	14.71	13.36	20/08/2003	800	88	−176.8
T, 458	23 08 25.75 −15 37 10	15.50	14.41	21/08/2003	3600	92	−178.5
R	23 08 29.46 −15 36 32	15.51	14.40	20,21/08/2003	3000	92	−175.5
K, 950	23 08 20.83 −15 36 20	15.77	14.72	22/08/2003	3600	105	−176.9

[a]Alphabetical identifications are from Buonanno *et al.* (1987), numerical ones are from Cuffey (1961).

[b]Our photometry from ANDICAM images.

[c]Signal to noise ratio in the continuum near 5865 Å per 4 pixel spectral resolution element.

Table 2.   Stellar Parameters

ID[a]	T_{eff} (K)	$\log(g)$ (dex)	v_t (km/s)
H,231	4300	0.62	2.0
R	4650	1.18	2.0
T,458	4715	1.21	2.0
K,950	4750	1.33	2.0

[a]Identifications as in notes to Table 1.

Table 3.   Equivalent Widths

Ion	λ (Å)	χ_{exc} (eV)	$\log gf$ (dex)	231 (mÅ)	R (mÅ)	950 (mÅ)	458 (mÅ)
OI	6300.30	0.00	-9.78	30.0	23.5	13.5	27.3
OI	6363.78	0.02	-10.30	9.0	$\cdots$	8.0	9.5
NaI	5682.63	2.10	-0.70	46.0	32.1	8.0	16.0
NaI	5688.19	2.10	-0.42	61.0	49.6	15.0	28.5
NaI	6160.75	2.00	-1.23	18.5	$\cdots$	$\cdots$	$\cdots$
MgI	4703.00	4.34	-0.67	157.2	126.7	115.8	136.0
MgI	5528.40	4.34	-0.48	170.2	148.0	133.8	145.8
MgI	5711.09	4.34	-1.67	82.7	64.0	30.0	46.0
SiI	5690.43	4.93	-1.87	27.0	20.0	$\cdots$	23.5
SiI	5948.54	5.08	-1.23	42.0	36.0	33.0	27.0
SiI	6155.13	5.62	-0.76	24.0	20.0	17.0	31.0
SiI	6237.32	5.62	-1.01	15.0	$\cdots$	$\cdots$	$\cdots$
CaI	5512.99	2.93	-0.27	56.5	40.0	23.0	33.7
CaI	5581.96	2.52	-0.47	82.7	58.3	44.8	48.1
CaI	5588.75	2.52	0.44	133.4	116.7	95.3	103.0
CaI	5590.11	2.52	-0.71	80.7	61.1	46.7	46.9
CaI	5601.28	2.52	-0.44	77.3	68.3	49.0	41.5
CaI	6161.30	2.52	-1.03	49.2	24.0	$\cdots$	22.0
CaI	6162.17	1.90	-0.09	$\cdots$	145.4	132.0	148.0
CaI	6166.44	2.52	-1.05	51.3	31.0	11.0	25.5
CaI	6169.04	2.52	-0.54	72.5	54.5	35.9	43.0
CaI	6169.56	2.52	-0.27	93.8	65.6	46.7	61.2
CaI	6471.66	2.52	-0.59	83.6	61.9	38.2	50.8
CaI	6493.78	2.52	0.14	123.8	90.9	77.8	89.6
ScII	5526.79	1.77	0.13	94.7	88.6	78.2	82.6
ScII	5657.90	1.51	-0.50	93.4	76.1	66.6	72.7
ScII	5667.15	1.50	-1.24	54.0	41.3	31.0	32.0
ScII	5669.04	1.50	-1.12	60.8	45.0	34.8	44.8
ScII	5684.20	1.51	-1.08	77.0	41.0	36.0	51.0
ScII	6245.64	1.51	-1.13	56.9	35.0	32.2	34.4
ScII	6604.60	1.36	-1.48	57.2	34.0	19.0	45.0
TiI	4981.74	0.85	0.50	167.7	111.3	97.5	120.7
TiI	4999.51	0.83	0.25	157.4	113.0	86.3	106.4
TiI	5022.87	0.83	-0.43	107.2	71.0	41.8	62.3
TiI	5039.96	0.02	-1.13	148.0	94.4	73.6	75.7
TiI	5426.26	0.02	-3.01	33.7	$\cdots$	$\cdots$	$\cdots$
TiI	5471.20	1.44	-1.39	15.0	$\cdots$	$\cdots$	$\cdots$
TiI	5490.15	1.46	-0.93	34.7	$\cdots$	$\cdots$	$\cdots$
TiI	5644.14	2.27	0.05	41.0	$\cdots$	$\cdots$	$\cdots$
TiI	5662.16	2.32	-0.11	24.5	$\cdots$	$\cdots$	$\cdots$
TiI	5937.81	1.07	-1.89	16.4	$\cdots$	$\cdots$	$\cdots$
TiI	5941.75	1.05	-1.52	43.6	17.3	$\cdots$	14.0
TiI	5953.16	1.89	-0.33	41.1	$\cdots$	$\cdots$	$\cdots$
TiI	5978.54	1.87	-0.50	29.0	$\cdots$	$\cdots$	$\cdots$
TiI	6258.10	1.44	-0.35	75.0	37.3	25.4	35.7

Table 3—Continued

Ion	λ (Å)	χ_{exc} (eV)	$\log gf$ (dex)	231 (mÅ)	R (mÅ)	950 (mÅ)	458 (mÅ)
TiI	6261.10	1.43	-0.48	72.2	36.5	18.0	28.7
TiI	6303.76	1.44	-1.57	9.0	$\cdots$	$\cdots$	$\cdots$
TiI	6312.22	1.46	-1.55	9.5	$\cdots$	$\cdots$	$\cdots$
TiI	6743.12	0.90	-1.63	45.8	$\cdots$	$\cdots$	$\cdots$
TiII	4657.20	1.24	-2.32	84.0	97.0	59.3	83.9
TiII	4708.67	1.24	-2.37	96.8	81.8	71.1	87.7
TiII	4865.62	1.12	-2.81	75.0	84.0	52.7	64.1
TiII	5185.91	1.89	-1.46	98.0	85.9	74.8	81.9
TiII	5336.79	1.58	-1.63	121.0	105.0	93.2	105.4
VI	5670.85	1.08	-0.43	35.0	$\cdots$	$\cdots$	$\cdots$
VI	5703.57	1.05	-0.21	34.3	$\cdots$	$\cdots$	$\cdots$
VI	6081.44	1.05	-0.58	29.8	$\cdots$	$\cdots$	$\cdots$
VI	6090.22	1.08	-0.06	41.7	$\cdots$	$\cdots$	$\cdots$
VI	6199.20	0.29	-1.28	32.0	$\cdots$	$\cdots$	$\cdots$
VI	6251.82	0.29	-1.34	35.4	$\cdots$	$\cdots$	$\cdots$
VI	6274.64	0.27	-1.67	21.8	$\cdots$	$\cdots$	$\cdots$
VI	6285.14	0.28	-1.51	46.2	$\cdots$	$\cdots$	$\cdots$
CrI	5345.81	1.00	-0.97	134.1	104.3	75.4	85.6
CrI	5348.33	1.00	-1.29	115.8	74.5	54.7	63.9
CrI	5409.80	1.03	-0.71	169.5	126.0	88.8	106.9
CrI	5787.96	3.32	-0.08	12.0	$\cdots$	$\cdots$	$\cdots$
MnI	4754.04	2.28	-0.09	107.2	74.2	49.8	62.2
MnI	4783.42	2.30	0.04	121.2	95.0	69.2	72.9
MnI	4823.51	2.32	0.14	116.5	75.0	67.5	78.0
MnI	5537.74	2.19	-2.02	28.0	$\cdots$	$\cdots$	$\cdots$
FeI	4788.77	3.24	-1.81	49.5	$\cdots$	$\cdots$	$\cdots$
FeI	4891.50	2.85	-0.11	170.7	144.8	137.7	142.3
FeI	4919.00	2.86	-0.34	168.5	141.0	117.4	141.4
FeI	5083.34	0.96	-2.96	165.2	131.2	112.3	126.2
FeI	5166.28	0.00	-4.20	$\cdots$	141.4	118.9	139.7
FeI	5194.95	1.56	-2.09	174.6	130.3	121.0	129.1
FeI	5232.95	2.94	-0.10	172.0	139.0	129.6	139.5
FeI	5324.19	3.21	-0.10	160.4	135.8	117.7	125.8
FeI	5393.18	3.24	-0.72	114.4	93.0	81.8	86.1
FeI	5410.92	4.47	0.40	87.1	73.4	56.0	68.3
FeI	5415.21	4.39	0.64	105.0	91.0	66.4	86.9
FeI	5424.08	4.32	0.51	114.7	87.8	83.1	99.2
FeI	5445.05	4.39	-0.03	79.3	70.0	47.0	67.2
FeI	5473.90	4.15	-0.69	42.2	43.9	20.0	24.5
FeI	5493.50	4.10	-1.68	15.9	$\cdots$	$\cdots$	$\cdots$
FeI	5497.52	1.01	-2.83	$\cdots$	147.7	134.3	143.9
FeI	5501.46	0.96	-3.05	$\cdots$	138.6	118.5	136.5
FeI	5506.79	0.99	-2.79	$\cdots$	146.2	130.0	142.4
FeI	5525.55	4.23	-1.08	21.0	$\cdots$	$\cdots$	13.5
FeI	5554.88	4.55	-0.35	33.9	35.0	22.0	25.6

Table 3—Continued

Ion	λ (Å)	χ_{exc} (eV)	$\log gf$ (dex)	231 (mÅ)	R (mÅ)	950 (mÅ)	458 (mÅ)
FeI	5567.39	2.61	-2.67	64.8	39.0	$\cdots$	31.2
FeI	5569.62	3.42	-0.49	123.0	92.0	81.1	91.2
FeI	5572.84	3.40	-0.28	146.1	108.6	100.1	104.3
FeI	5576.09	3.43	-0.92	109.1	83.5	63.7	72.3
FeI	5586.76	3.37	-0.14	144.8	117.7	105.1	114.1
FeI	5641.44	4.26	-1.08	30.0	$\cdots$	$\cdots$	$\cdots$
FeI	5662.52	4.18	-0.57	65.0	48.5	37.2	39.8
FeI	5679.02	4.65	-0.82	25.0	$\cdots$	$\cdots$	$\cdots$
FeI	5701.54	2.56	-2.14	106.0	76.3	46.9	66.7
FeI	5705.98	4.61	-0.49	25.5	$\cdots$	$\cdots$	29.0
FeI	5752.04	4.55	-0.94	19.2	$\cdots$	$\cdots$	$\cdots$
FeI	5753.12	4.26	-0.69	52.5	38.9	30.0	30.4
FeI	5762.99	4.21	-0.41	70.2	44.9	36.5	48.0
FeI	5775.06	4.22	-1.30	22.6	$\cdots$	$\cdots$	$\cdots$
FeI	5778.46	2.59	-3.43	19.6	$\cdots$	$\cdots$	$\cdots$
FeI	5806.72	4.61	-0.95	11.0	$\cdots$	$\cdots$	$\cdots$
FeI	5859.60	4.55	-0.55	34.0	22.0	15.6	17.7
FeI	5862.35	4.55	-0.33	52.2	30.0	21.0	24.2
FeI	5883.81	3.96	-1.26	27.0	17.5	$\cdots$	19.0
FeI	5930.17	4.65	-0.14	47.4	36.7	21.3	18.0
FeI	5934.65	3.93	-1.07	42.0	42.0	29.5	21.8
FeI	5952.72	3.98	-1.34	53.3	35.5	20.0	24.3
FeI	5956.69	0.86	-4.50	110.7	60.7	34.5	51.2
FeI	5976.79	3.94	-1.33	41.7	18.0	17.5	19.3
FeI	5983.69	4.55	-0.66	37.5	$\cdots$	16.8	20.0
FeI	6024.05	4.55	0.03	67.4	40.5	38.9	48.9
FeI	6027.05	4.07	-1.09	38.3	$\cdots$	$\cdots$	$\cdots$
FeI	6055.99	4.73	-0.37	29.2	28.0	$\cdots$	15.0
FeI	6065.48	2.61	-1.41	143.9	111.4	90.6	97.2
FeI	6078.50	4.79	-0.33	29.2	25.5	10.5	12.5
FeI	6137.69	2.59	-1.35	144.3	110.6	99.2	109.8
FeI	6151.62	2.18	-3.37	66.0	37.8	17.6	30.1
FeI	6157.73	4.07	-1.16	42.5	26.2	8.0	20.9
FeI	6165.36	4.14	-1.47	24.9	$\cdots$	$\cdots$	$\cdots$
FeI	6173.34	2.22	-2.88	91.0	62.6	36.0	51.6
FeI	6180.20	2.73	-2.65	55.0	29.8	14.0	27.7
FeI	6187.99	3.94	-1.62	14.0	$\cdots$	$\cdots$	$\cdots$
FeI	6191.56	2.43	-1.42	174.9	129.4	99.3	128.8
FeI	6200.31	2.61	-2.37	88.5	59.7	31.5	47.1
FeI	6240.65	2.22	-3.17	59.3	35.2	16.0	23.0
FeI	6246.32	3.60	-0.88	91.9	74.3	48.9	57.7
FeI	6252.55	2.40	-1.77	146.8	106.8	100.0	112.0
FeI	6254.26	2.28	-2.43	122.1	95.9	73.0	79.3
FeI	6265.13	2.18	-2.54	118.9	89.8	59.1	77.7
FeI	6297.79	2.22	-2.64	108.1	79.9	44.1	59.4

Table 3—Continued

Ion	λ (Å)	χ_{exc} (eV)	$\log gf$ (dex)	231 (mÅ)	R (mÅ)	950 (mÅ)	458 (mÅ)
FeI	6301.51	3.65	−0.72	93.7	71.0	50.0	65.1
FeI	6315.31	4.14	−1.23	25.0	$\cdots$	$\cdots$	$\cdots$
FeI	6355.03	2.84	−2.29	69.3	45.1	19.0	33.0
FeI	6380.75	4.19	−1.38	22.3	$\cdots$	$\cdots$	$\cdots$
FeI	6393.60	2.43	−1.58	156.6	118.3	100.8	115.0
FeI	6408.03	3.69	−1.02	86.7	59.3	40.2	49.6
FeI	6411.65	3.65	−0.72	109.2	75.1	58.2	75.7
FeI	6421.35	2.28	−2.01	145.9	101.0	85.7	101.2
FeI	6475.63	2.56	−2.94	58.8	33.2	14.6	19.5
FeI	6481.87	2.28	−3.01	86.3	46.5	30.6	43.2
FeI	6498.94	0.96	−4.69	98.1	51.2	31.9	43.5
FeI	6546.24	2.76	−1.54	137.2	99.1	74.1	92.7
FeI	6581.21	1.48	−4.68	42.7	$\cdots$	$\cdots$	$\cdots$
FeI	6592.91	2.73	−1.47	130.9	97.4	81.7	90.8
FeI	6593.87	2.43	−2.37	99.2	67.4	48.0	64.2
FeI	6608.02	2.28	−3.93	16.0	$\cdots$	$\cdots$	$\cdots$
FeI	6609.11	2.56	−2.66	79.1	45.5	26.5	37.5
FeI	6633.75	4.79	−0.80	27.0	$\cdots$	$\cdots$	12.0
FeI	6648.12	1.01	−5.92	13.0	$\cdots$	$\cdots$	$\cdots$
FeI	6739.52	1.56	−4.79	27.0	$\cdots$	$\cdots$	$\cdots$
FeI	6750.15	2.42	−2.58	101.8	68.0	46.6	60.2
FeI	6839.83	2.56	−3.35	27.9	$\cdots$	$\cdots$	$\cdots$
FeI	6843.65	4.55	−0.83	25.6	$\cdots$	$\cdots$	$\cdots$
FeI	6855.18	4.56	−0.74	34.6	$\cdots$	$\cdots$	$\cdots$
FeI	6861.95	2.42	−3.85	20.0	$\cdots$	$\cdots$	$\cdots$
FeI	6978.85	2.48	−2.45	104.8	72.6	44.6	66.5
FeI	6988.52	2.40	−3.56	39.7	$\cdots$	$\cdots$	$\cdots$
FeI	7022.95	4.19	−1.15	38.0	$\cdots$	$\cdots$	$\cdots$
FeI	7038.22	4.22	−1.20	30.1	$\cdots$	$\cdots$	$\cdots$
FeII	4923.93	2.88	−1.32	138.4	$\cdots$	$\cdots$	$\cdots$
FeII	5197.58	3.23	−2.23	74.0	64.0	70.9	76.8
FeII	5234.63	3.22	−2.22	75.1	67.6	74.3	83.6
FeII	5414.08	3.22	−3.62	22.0	23.5	10.0	16.5
FeII	5425.26	3.00	−3.24	29.0	27.0	27.0	37.5
FeII	5534.85	3.25	−2.64	64.3	56.8	53.2	52.9
FeII	5991.38	3.15	−3.57	30.0	$\cdots$	12.0	27.4
FeII	6149.26	3.89	−2.69	18.0	25.2	16.4	26.9
FeII	6247.56	3.89	−2.36	40.0	31.9	31.0	31.6
FeII	6369.46	2.89	−4.20	10.0	$\cdots$	$\cdots$	$\cdots$
FeII	6416.92	3.89	−2.69	19.0	15.9	$\cdots$	15.8
FeII	6516.08	2.89	−3.45	64.0	58.3	47.5	51.8
CoI	5530.79	1.71	−2.06	30.0	$\cdots$	9.0	10.0
CoI	5647.23	2.28	−1.56	21.5	$\cdots$	$\cdots$	$\cdots$
CoI	6189.00	1.71	−2.45	18.0	$\cdots$	$\cdots$	$\cdots$
NiI	5578.72	1.68	−2.64	86.1	44.1	32.0	33.0

Table 3—Continued

Ion	λ (Å)	χ_{exc} (eV)	$\log gf$ (dex)	231 (mÅ)	R (mÅ)	950 (mÅ)	458 (mÅ)
NiI	5587.86	1.93	−2.14	81.4	36.9	20.5	39.0
NiI	5682.20	4.10	−0.47	18.0	⋯	⋯	⋯
NiI	5748.35	1.68	−3.26	41.0	⋯	7.0	14.0
NiI	5846.99	1.68	−3.21	34.1	⋯	⋯	⋯
NiI	6128.97	1.68	−3.33	30.0	23.5	10.4	10.5
NiI	6175.37	4.09	−0.54	22.0	⋯	⋯	⋯
NiI	6176.81	4.09	−0.53	21.8	⋯	⋯	⋯
NiI	6177.24	1.83	−3.51	15.0	⋯	⋯	⋯
NiI	6482.80	1.93	−2.63	47.8	21.0	13.3	19.6
NiI	6586.31	1.95	−2.81	45.5	22.3	8.0	13.0
NiI	6643.63	1.68	−2.30	126.3	83.0	56.5	73.9
NiI	6767.77	1.83	−2.17	106.4	74.8	51.7	64.1
CuI	5105.54	1.39	−1.50	82.0	46.0	24.0	28.0
CuI	5782.12	1.64	−1.78	41.5	⋯	⋯	⋯
ZnI	4722.16	4.03	−0.39	45.0	36.6	41.0	44.0
ZnI	4810.54	4.08	−0.17	46.0	54.6	52.4	48.5
YII	4883.69	1.08	0.07	85.0	71.3	74.5	71.8
YII	5087.43	1.08	−0.17	71.0	55.0	56.2	60.1
YII	5200.42	0.99	−0.57	56.0	42.1	32.7	44.0
ZrI	6127.44	0.15	−1.06	17.0	⋯	⋯	⋯
ZrI	6134.55	0.00	−1.28	13.0	⋯	⋯	⋯
ZrI	6143.20	0.07	−1.10	10.0	⋯	⋯	⋯
BaII	5853.70	0.60	−1.01	117.3	98.1	99.9	108.2
BaII	6141.70	0.70	−0.07	172.8	134.7	152.3	155.9
BaII	6496.90	0.60	−0.38	186.6	146.8	154.9	163.0
LaII	5122.99	0.32	−0.85	27.8	⋯	⋯	⋯
LaII	6390.48	0.32	−1.41	21.5	⋯	⋯	⋯
NdII	4947.02	0.56	−1.13	18.0	⋯	⋯	⋯
NdII	4959.12	0.06	−0.80	66.6	34.0	23.5	32.0
NdII	5092.79	0.38	−0.61	44.0	28.5	17.4	16.9
NdII	5212.35	0.20	−0.96	48.0	⋯	⋯	⋯
NdII	5249.58	0.98	0.20	49.9	30.5	33.5	31.5
NdII	5319.81	0.55	−0.14	61.9	33.2	33.8	27.8
EuII	6645.11	1.38	0.12	25.5	⋯	⋯	⋯

Table 4.   Adopted Solar Abundances

Element	[X/H][a]	Element	[X/H][a]
O	8.85	Fe	7.45
Na	6.33	Ni	6.25
Mg	7.54	Cu	4.21
Al	6.47	Zn	4.60
Si	7.55	Ba	2.13
Ca	6.36	Y	2.24
Sc	3.10	Zr	2.60
Ti	4.99	La	1.14
V	4.00	Nd	1.45
Cr	5.67	Eu	0.51
Mn	5.39	Dy	1.10

[a]Given on a scale where $\log(N(H))=12.0$; values in dex.

Table 5a.   Abundance Ratios: O to Mg

Star	[Fe/H]$_I$ $\pm\sigma/\sqrt{N}$ (dex)	N	[Fe/H]$_{II}$ $\pm\sigma/\sqrt{N}$ (dex)	N	[O/Fe] $\pm\sigma/\sqrt{N}$ (dex)	N	[Na/Fe] $\pm\sigma/\sqrt{N}$ (dex)	N	[Mg/Fe] $\pm\sigma/\sqrt{N}$ (dex)	N
231	-1.76 ± 0.05*	90	-1.72 ± 0.06	12	0.26 ± 0.05*	2	0.10 ± 0.05	3	0.67 ± 0.16	3
R	-1.77 ± 0.05*	66	-1.80 ± 0.08	9	0.49 ± 0.10	1	0.19 ± 0.05*	2	0.52 ± 0.06	3
458	-1.79 ± 0.05*	70	-1.77 ± 0.05	10	0.55 ± 0.05*	2	-0.10 ± 0.05*	2	0.55 ± 0.20	3
950	-1.94 ± 0.05*	64	-1.88 ± 0.05	9	0.52 ± 0.15	2	-0.28 ± 0.05*	2	0.45 ± 0.20	3

*The minimum value of 0.05 dex has been adopted, the nominal calculated value is smaller.

Table 5b.   Abundance Ratios: Si to V

Star	[Si/Fe] $\pm\sigma/\sqrt{N}$ (dex)	N	[Ca/Fe] $\pm\sigma/\sqrt{N}$ (dex)	N	[Sc/Fe] $\pm\sigma/\sqrt{N}$ (dex)	N	[Ti/Fe] $\pm\sigma/\sqrt{N}$ (dex)	N	[V/Fe] $\pm\sigma/\sqrt{N}$ (dex)	N
231	0.33 ± 0.09	4	$0.09 \pm 0.05^*$	11	0.20 ± 0.07	7	$0.16 \pm 0.05^*$	18	-0.07 ± 0.06	8
R	0.36 ± 0.10	3	$0.11 \pm 0.05^*$	12	$0.09 \pm 0.05^*$	7	0.12 ± 0.08	7	$\cdots$	0
458	0.45 ± 0.12	3	$0.05 \pm 0.05^*$	12	0.10 ± 0.06	7	0.18 ± 0.07	7	$\cdots$	0
950	0.42 ± 0.11	2	0.07 ± 0.05	11	$0.15 \pm 0.05^*$	7	$0.07 \pm 0.05^*$	6	$\cdots$	0

*The minimum value of 0.05 dex has been adopted; the nominal calculated value is smaller.

Table 5c.   Abundance Ratios: Cr to Cu

Star	[Cr/Fe] $\pm\sigma/\sqrt{N}$ (dex)	N	[Mn/Fe] $\pm\sigma/\sqrt{N}$ (dex)	N	[Co/Fe] $\pm\sigma/\sqrt{N}$ (dex)	N	[NiFe] $\pm\sigma/\sqrt{N}$ (dex)	N	[Cu/Fe] $\pm\sigma/\sqrt{N}$ (dex)	N
231	-0.24 ± 0.09	4	-0.24 ± 0.09	4	$0.11 \pm 0.05^*$	3	$-0.06 \pm 0.05^*$	13	-0.63 ± 0.06	2
R	-0.16 ± 0.11	3	-0.48 ± 0.13	3	$\cdots$	0	-0.07 ± 0.08	7	-0.57 ± 0.10	1
458	-0.29 ± 0.06	3	$-0.43 \pm 0.05^*$	3	0.18 ± 0.10	1	$-0.09 \pm 0.05^*$	8	-0.72 ± 0.10	1
950	$-0.29 \pm 0.05^*$	3	-0.39 ± 0.08	3	0.32 ± 0.10	1	-0.09 ± 0.06	8	-0.62 ± 0.10	1

*The minimum value of 0.05 dex has been adopted; the nominal calculated value is smaller.

Table 5d.   Abundance Ratios: Zn to La

Star	[Zn/Fe] $\pm\sigma/\sqrt{N}$ (dex)	N	[Y/Fe] $\pm\sigma/\sqrt{N}$ (dex)	N	[Zr/Fe] $\pm\sigma/\sqrt{N}$ (dex)	N	[Ba/Fe] $\pm\sigma/\sqrt{N}$ (dex)	N	[La/Fe] $\pm\sigma/\sqrt{N}$ (dex)	N
231	-0.09 ± 0.08	2	$-0.29 \pm 0.05^*$	4	0.36 ± 0.10	3	0.24 ± 0.10	3	0.12 ± 0.16	2
R	-0.09 ± 0.08	2	$-0.35 \pm 0.05^*$	4	$\cdots$	0	0.05 ± 0.09	3	$\cdots$	0
458	-0.16 ± 0.05	2	-0.31 ± 0.06	4	$\cdots$	0	0.34 ± 0.07	3	$\cdots$	0
950	$0.13 \pm 0.05^*$	2	-0.11 ± 0.08	4	$\cdots$	0	0.50 ± 0.08	3	$\cdots$	0

*The minimum value of 0.05 dex has been adopted; the nominal calculated value is smaller.

Table 5e.   Abundance Ratios: Nd to Eu

Star	[Nd/Fe] $\pm\sigma/\sqrt{N}$ (dex)	N	[Eu/Fe] $\pm\sigma/\sqrt{N}$ (dex)	N
231	$0.40 \pm 0.05^*$	6	0.61 ± 0.10	1
R	$0.26 \pm 0.05^*$	4	$\cdots$	0
458	0.19 ± 0.07	4	$\cdots$	0
950	0.41 ± 0.08	4	$\cdots$	0

*The minimum value of 0.05 dex has been adopted; the nominal calculated value is smaller.

Table 6.   Mean Abundances and Spread Ratios

Species	Mean Abund. [X/Fe] (dex)	σ (dex)	σ(tot) (dex)	Spread Ratio[a] (dex)	No. of Stars[e]
OI	0.46	0.13	0.10	1.30	4
NaI	−0.02	0.21	0.07	3.00	4
MgI	0.55	0.09	0.20	0.45	4
SiI	0.39	0.06	0.10	0.60	4
CaI	0.08	0.03	0.12	0.25	4
ScII	0.14	0.05	0.21	0.24	4
TiI	0.13	0.05	0.12	0.42	4
TiII	0.34	0.06	0.15	0.40	4
VI	−0.07	$\cdots$	0.23	$\cdots$	1
CrI	−0.25	0.06	0.17	0.35	4
MnI	−0.39	0.10	0.18	0.55	4
FeI	−1.82	0.08	0.10	0.80	4
FeII	−1.79	0.07	0.13	0.54	4
CoI	0.20	0.11	0.12	0.92	3
NiI	−0.08	0.02	0.10	0.20	4
CuI	−0.64	0.06	0.16	0.38	4
ZnI	−0.03	0.11	0.13	0.85	4
YII	−0.27	0.11	0.15	0.73	4
ZrI	0.36	$\cdots$	0.16	$\cdots$	1
BaII	0.28	0.19	0.22	0.86	4
LaII	0.12	$\cdots$	0.18	$\cdots$	1
NdII	0.32	0.11	0.11	1.00	4
EuII	0.61	$\cdots$	$\cdots$	$\cdots$	1

[a]This is the ratio of σ to σ(tot). See text.

[e]The number of stars in which lines of this species were detected.

Table 7. Comparison of Abundance Ratios in NGC 7492 to Those in M3 and M13

Species	Mean Abund. NGC 7492 [X/Fe] (dex)	σ (dex)	Δ[X/Fe] (NGC 7492–M3/M13) (dex)	[X/Fe] Corr.[a] (dex)
O	0.46	0.15	0.02	$\cdots$
Na	−0.02	0.21	−0.10	0.00
Mg	0.55	0.09	0.12	0.05
Si	0.39	0.06	0.23	0.08
Ca	0.08	0.03	−0.09	0.07
Sc	0.14	0.05	0.14	0.07
Ti	0.24	0.06	0.08	0.07
V	−0.07	$\cdots$	0.01	$\cdots$
Cr	−0.25	0.06	−0.22	−0.10
Mn	−0.39	0.10	−0.04	−0.05
Co	0.20	0.11	0.21	0.07
Ni	−0.08	0.01	−0.01	0.00
Cu	−0.64	0.06	−0.02	$\cdots$
Zn	−0.03	0.11	0.02	$\cdots$
Y	−0.27	0.11	−0.04	$\cdots$
Zr	0.36	$\cdots$	0.40	$\cdots$
Ba	0.28	0.019	0.05	−0.04
La	0.12	$\cdots$	0.03	$\cdots$
Nd	0.32	0.11	0.10	$\cdots$
Eu	0.61	$\cdots$	0.07	0.00

[a]This is the approximate correction to be added to the mean [X/Fe] in M3/M13 to take into account trends of [X/Fe] with [Fe/H] given the different metallicities of the clusters, i.e. it must be subtracted from Δ[X/Fe] to obtain $\Delta(cor)$[X/Fe].
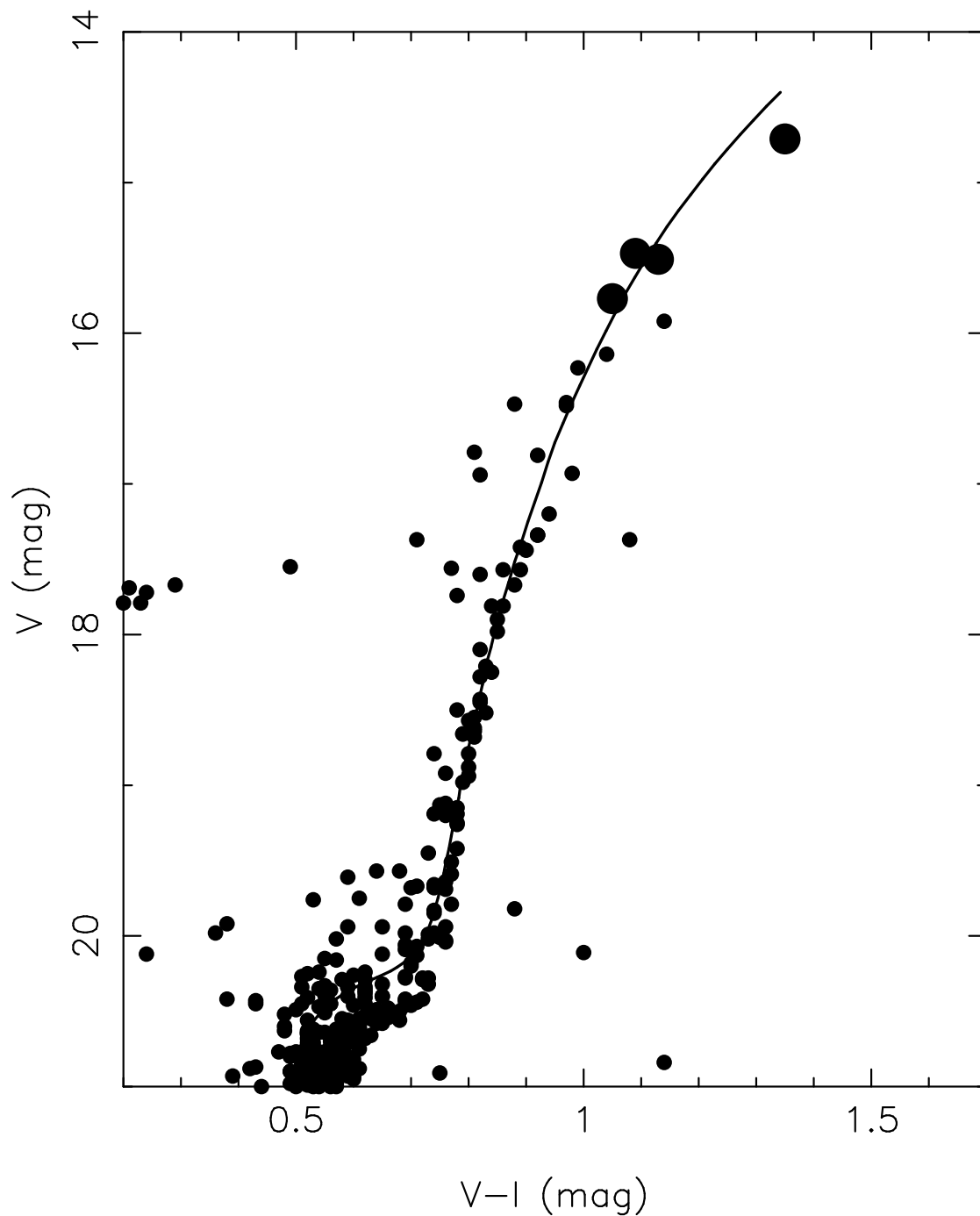
Fig. 1.— The $V - I$ CMD of NGC 7492: the four RGB stars observed with HIRES (big filled circles) are shown superposed on a 12 Gyr isochrone from Yi *et al.* (2001) with [Fe/H] -1.7 dex shifted to the distance of NGC 7492. The small circles denote stars from Buonanno *et al.* (1987) in this GC roughly transformed from B, V to V, I.
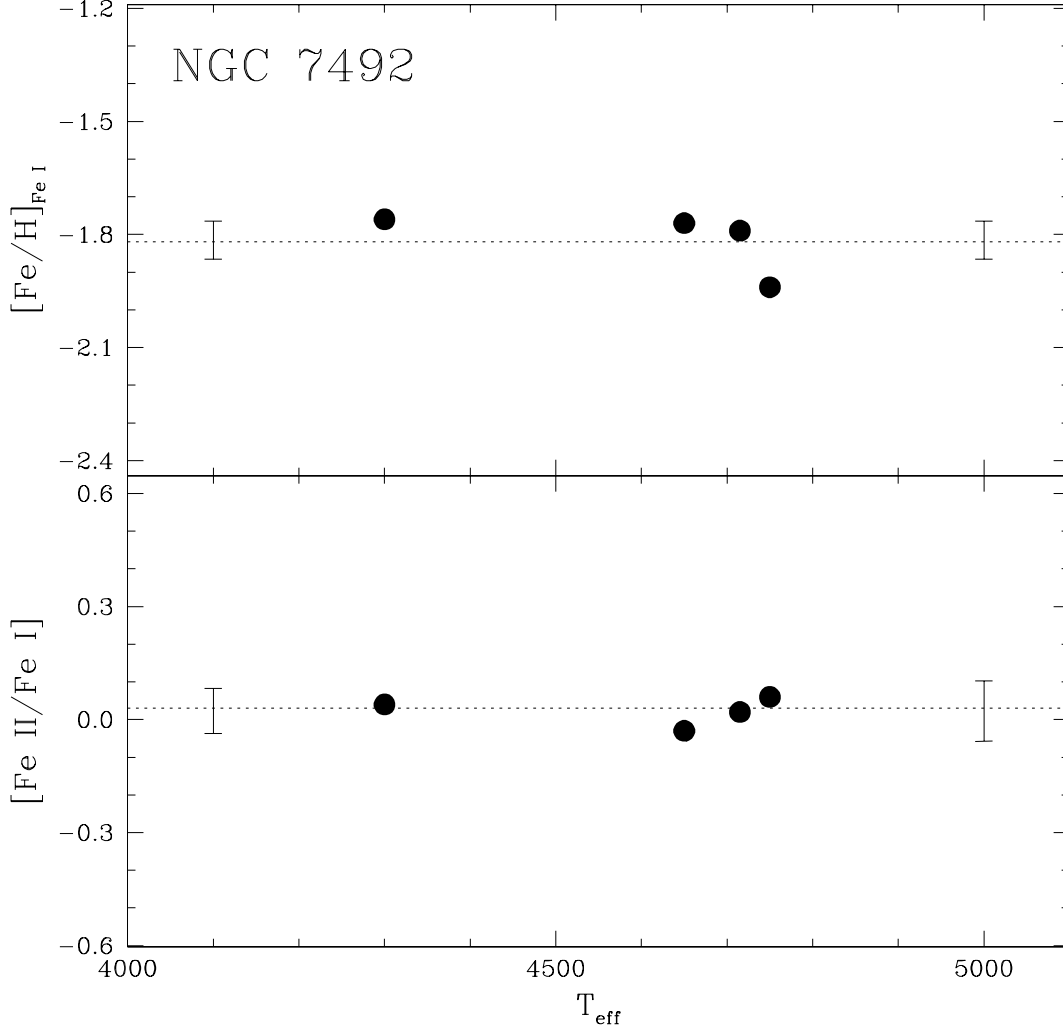
Fig. 2.— The [Fe/H] from lines of Fe I is shown as a function of T_{eff} in the upper panel, while the lower panel shows the ionization equilibrium of Fe for our sample of 4 stars in NGC 7492. The error bars on the left margin are those of the most luminous star, while the error bars on the right margin are those of the faintest star in our sample. The dotted horizontal line indicates the mean value for our sample in this GC.
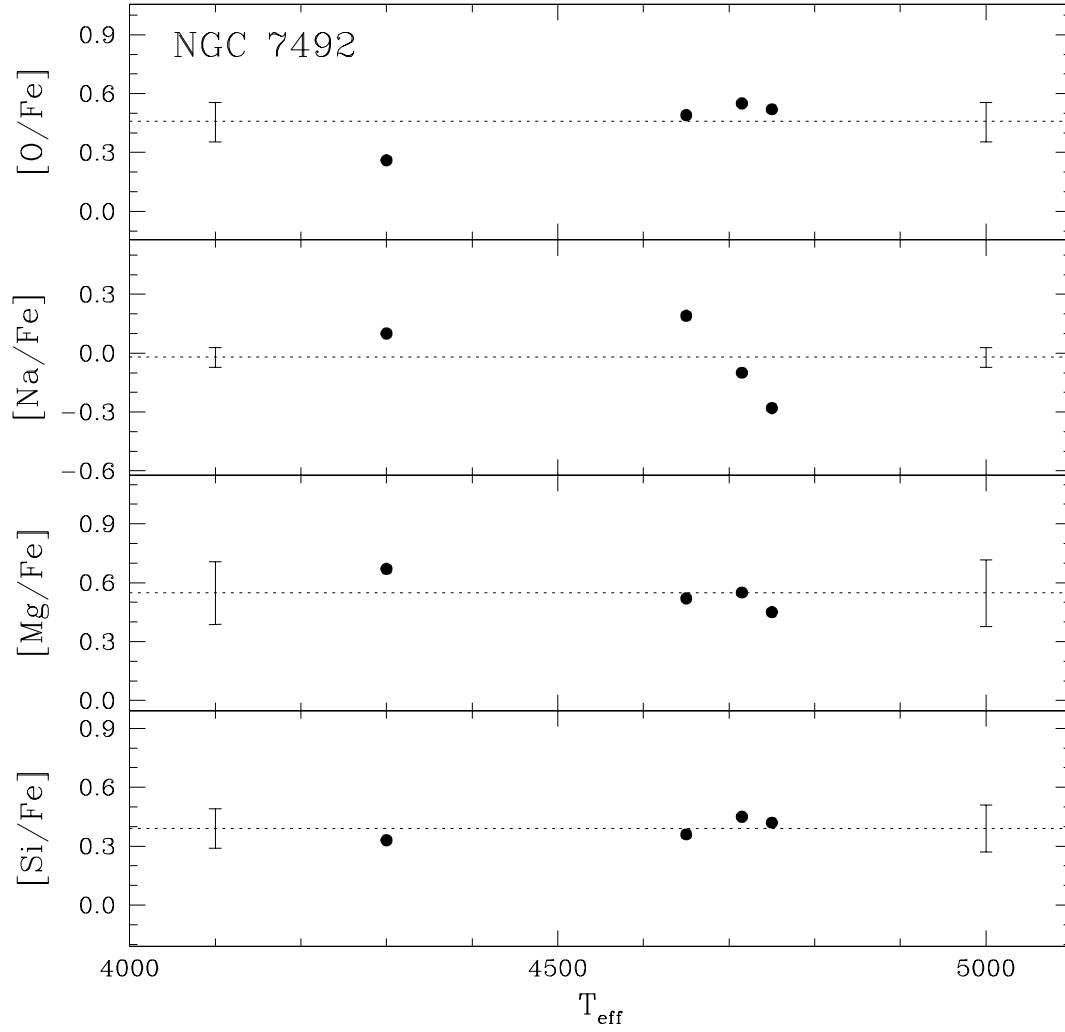
Fig. 3.— [X/Fe] for the elements O, Na, Mg and Si are shown as a function of T_{eff} for our sample of 4 stars in NGC 7492. The error bars for the most luminous and least luminous stars, as well as the cluster mean, are indicated as in Figure 2.
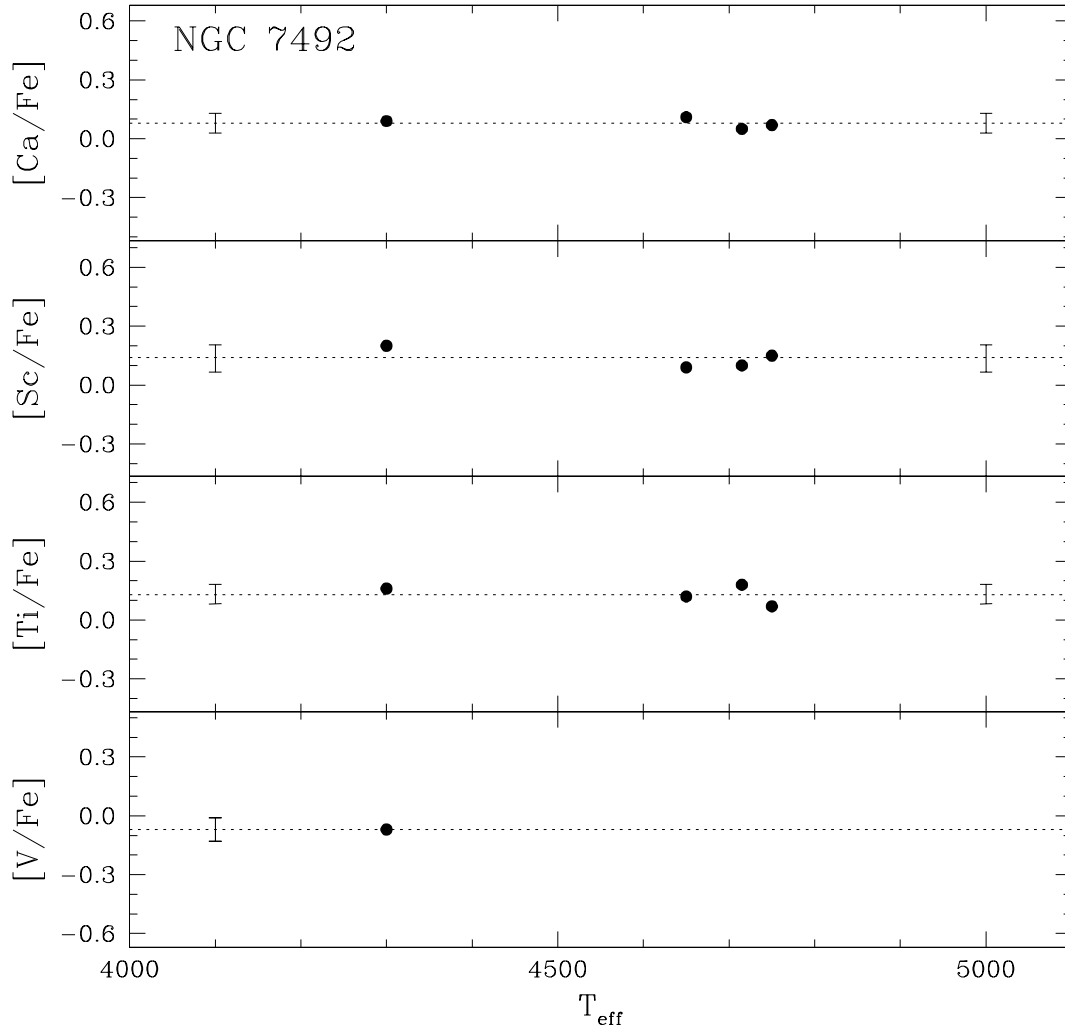
Fig. 4.— Same as Figure 3 for the elements Ca, Sc, Ti and V in NGC 7492.
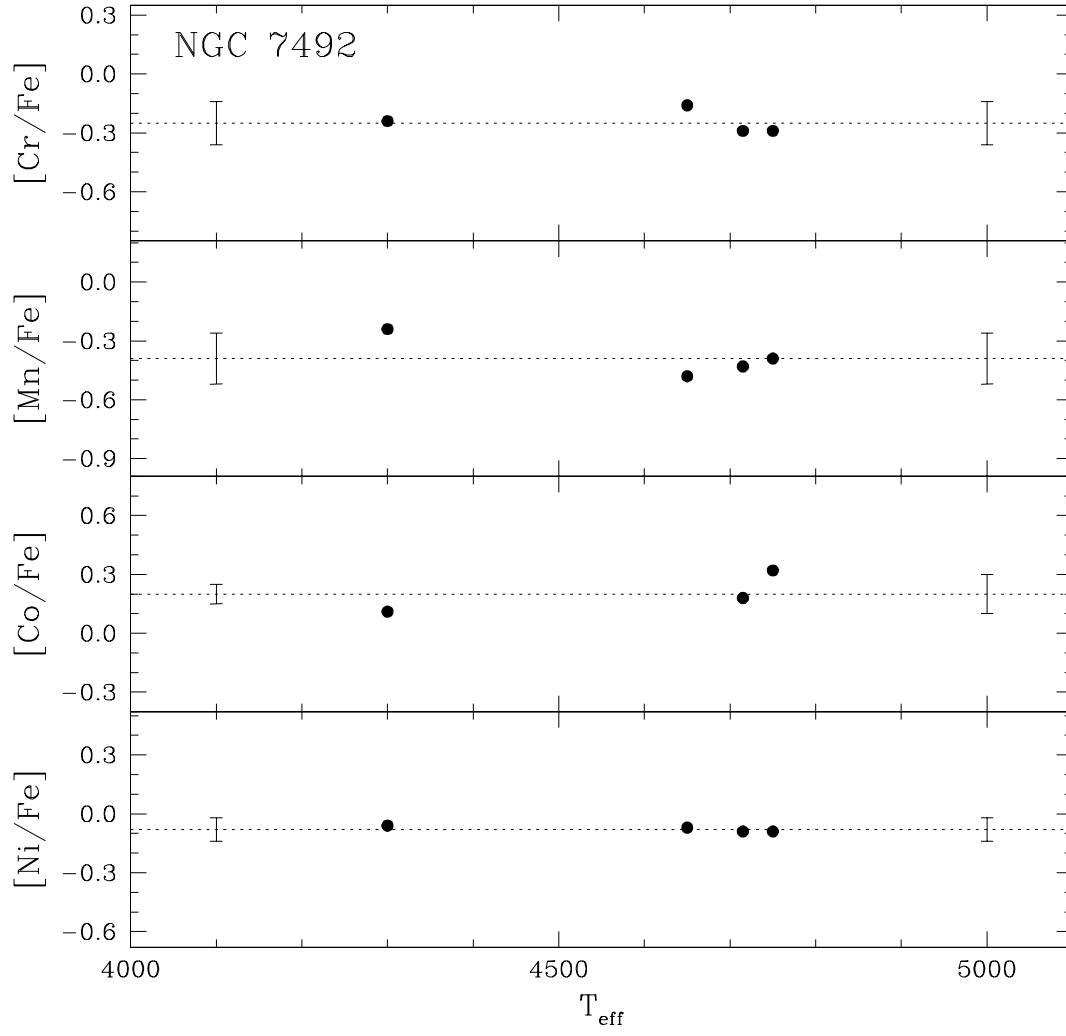
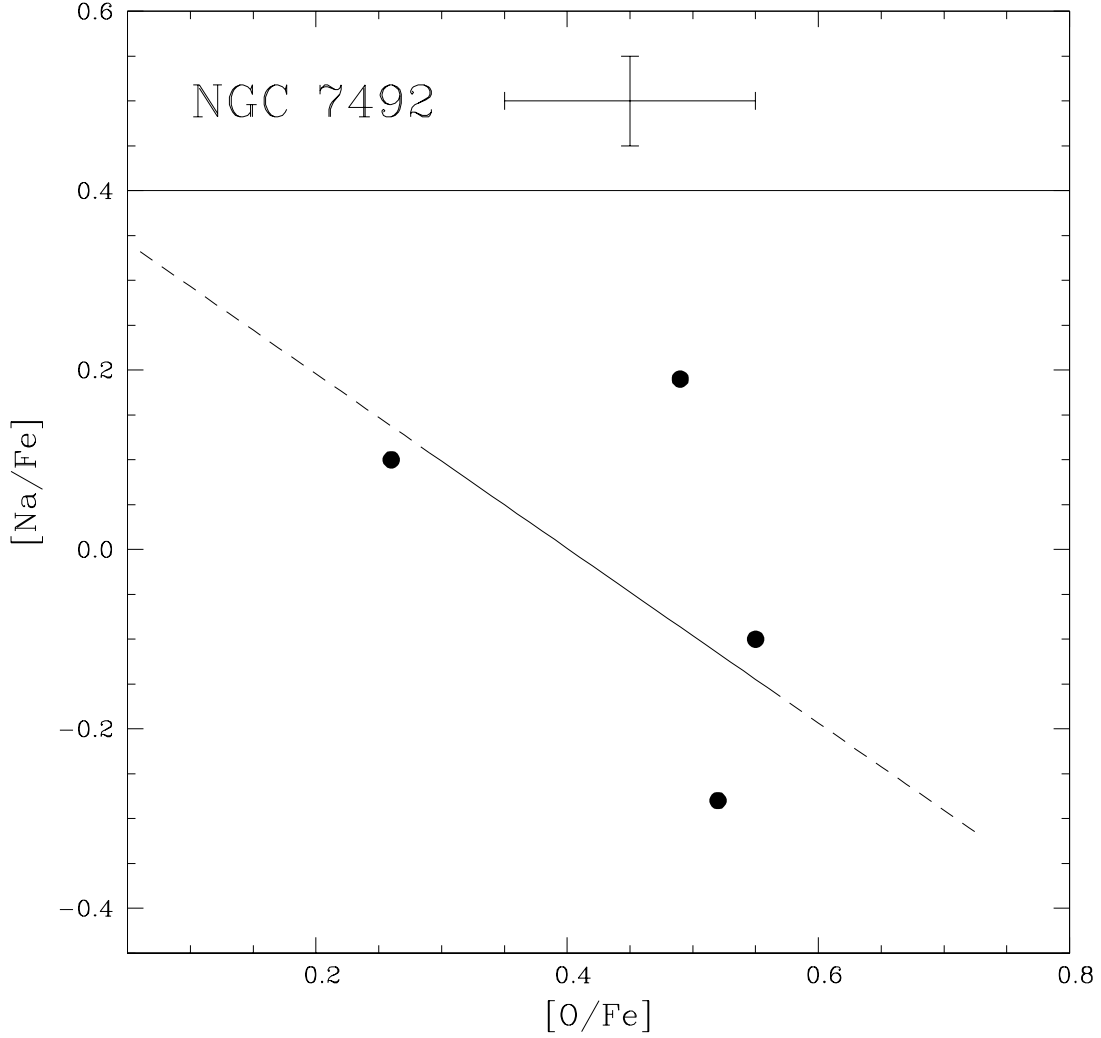Fig. 5.— Same as Figure 3 for the elements Cr, Mn, Co and Ni in NGC 7492.
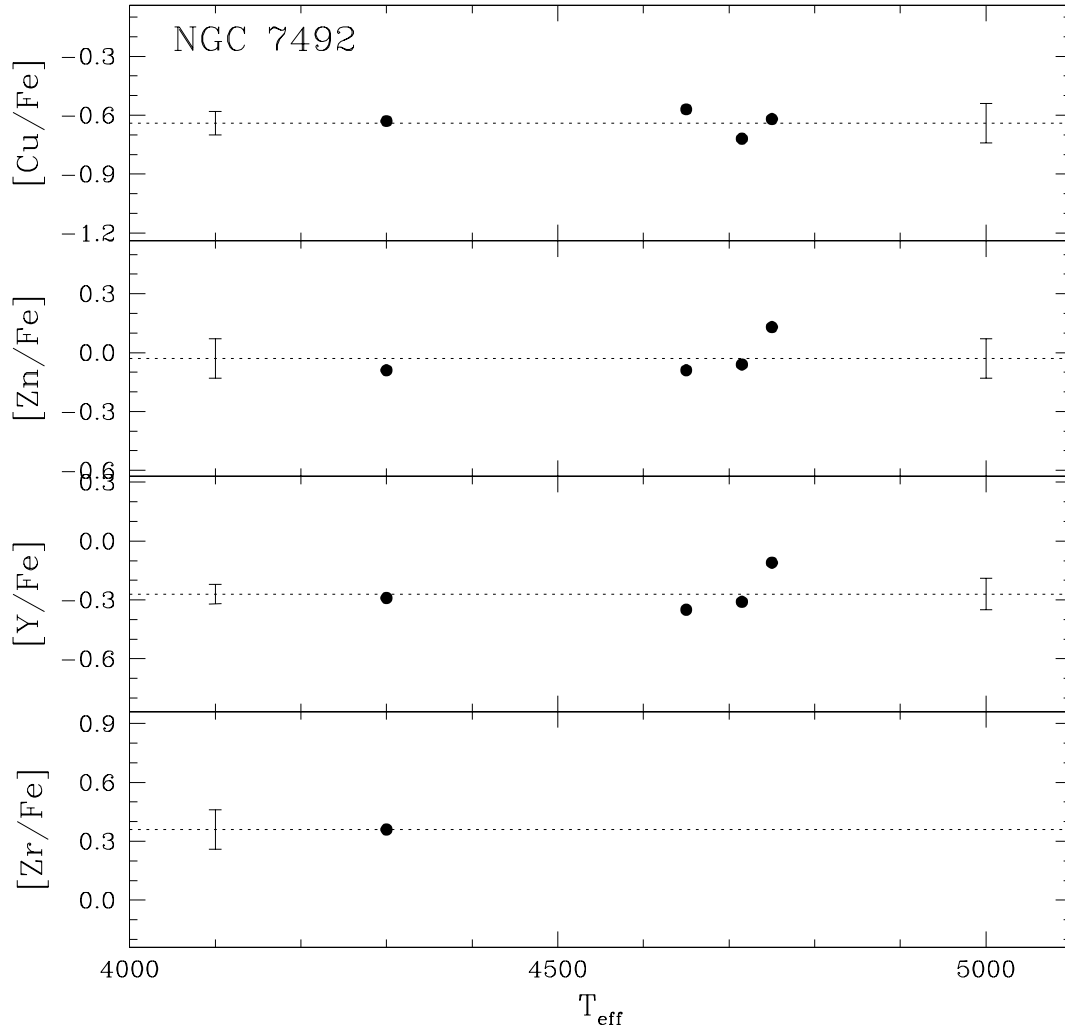
Fig. 6.— Same as Figure 3 for the elements Cu, Zn, Y and Zr in NGC 7492.
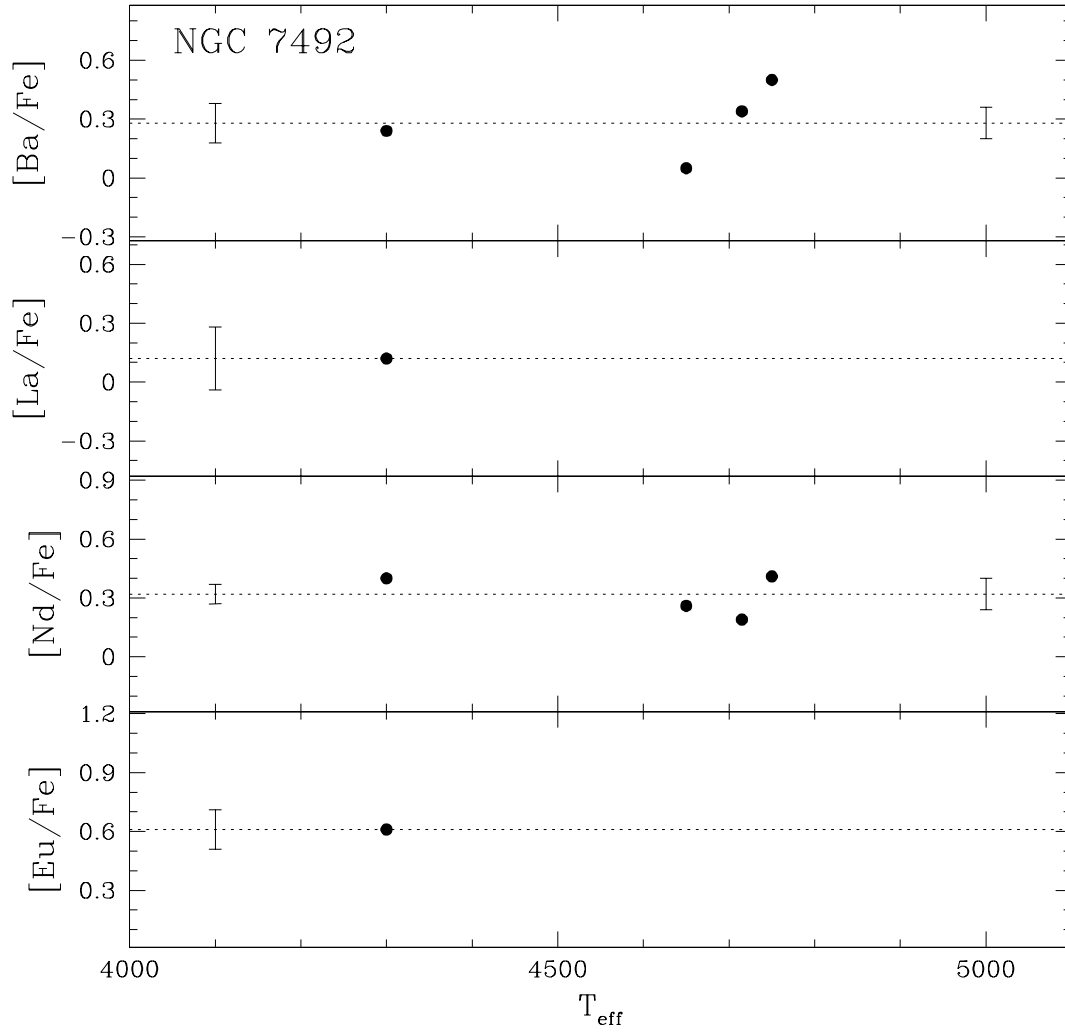
Fig. 7.— Same as Figure 3 for the elements Ba, La, Nd and Eu in NGC 7492.

Fig. 8.— The ratio [Na/Fe] is shown as a function of [O/Fe] for our sample of four stars in NGC 7492. The error bars typical of the most luminous and least luminous stars in our sample are indicated. The line represents the relationship found by Sneden *et al.* (2004), with a shift of −0.07 and +0.1 dex in the vertical and horizontal axis with respect to the relation we found for M13 (Cohen & Melendez 2005); the line is solid between the first and third quartiles of Sneden *et al.* (2004) M3 sample and is dashed outside that regime.
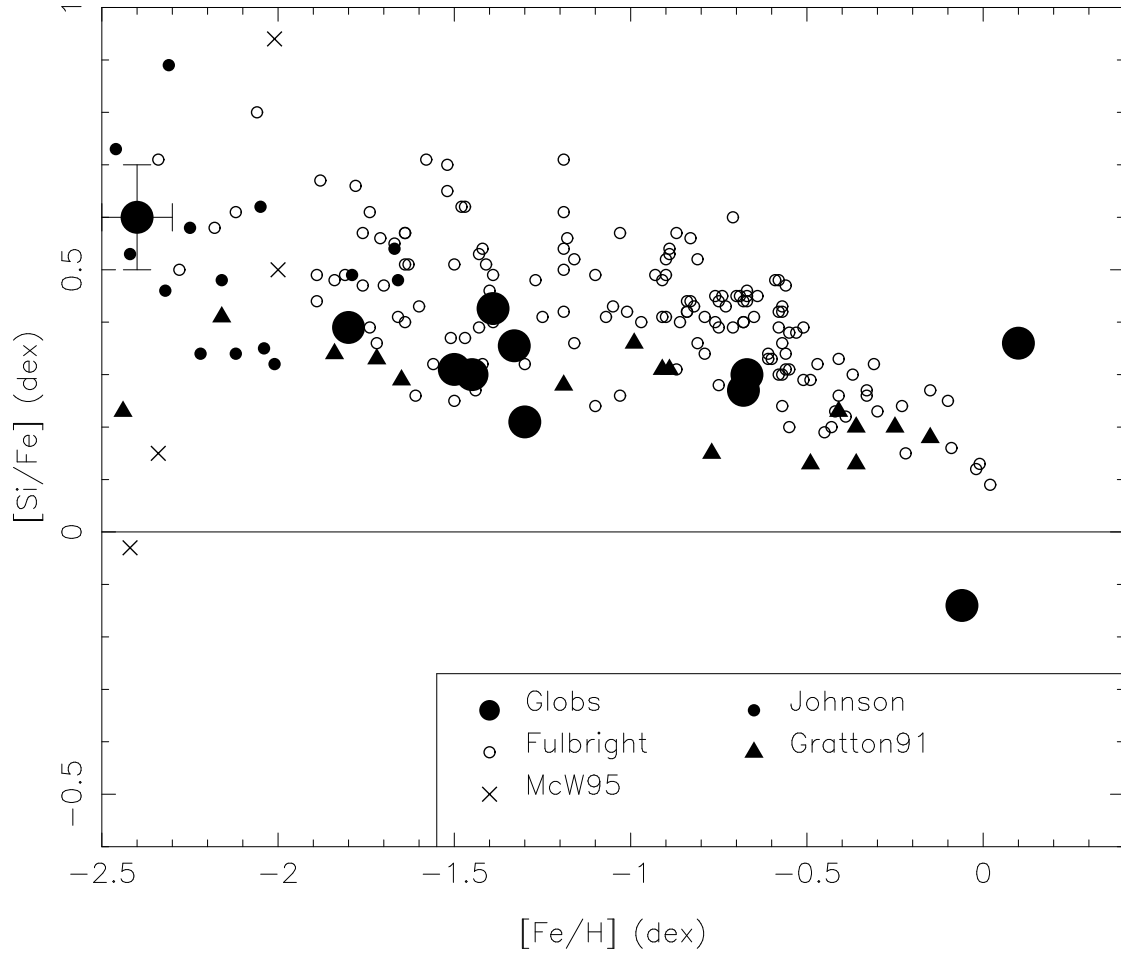
Fig. 9.— The abundance ratio [Si/Fe] is shown as a function of [Fe/H] for a sample of 13 Galactic GCs (see text for references), indicated as large filled circles. This is compared to the same relationship for halo field stars from surveys by Fulbright (2000), McWilliam *et al.* (1995), Johnson (2002) and Gratton & Sneden (1991). An error bar typical of the GCs is shown for the lowest metallicity GC.
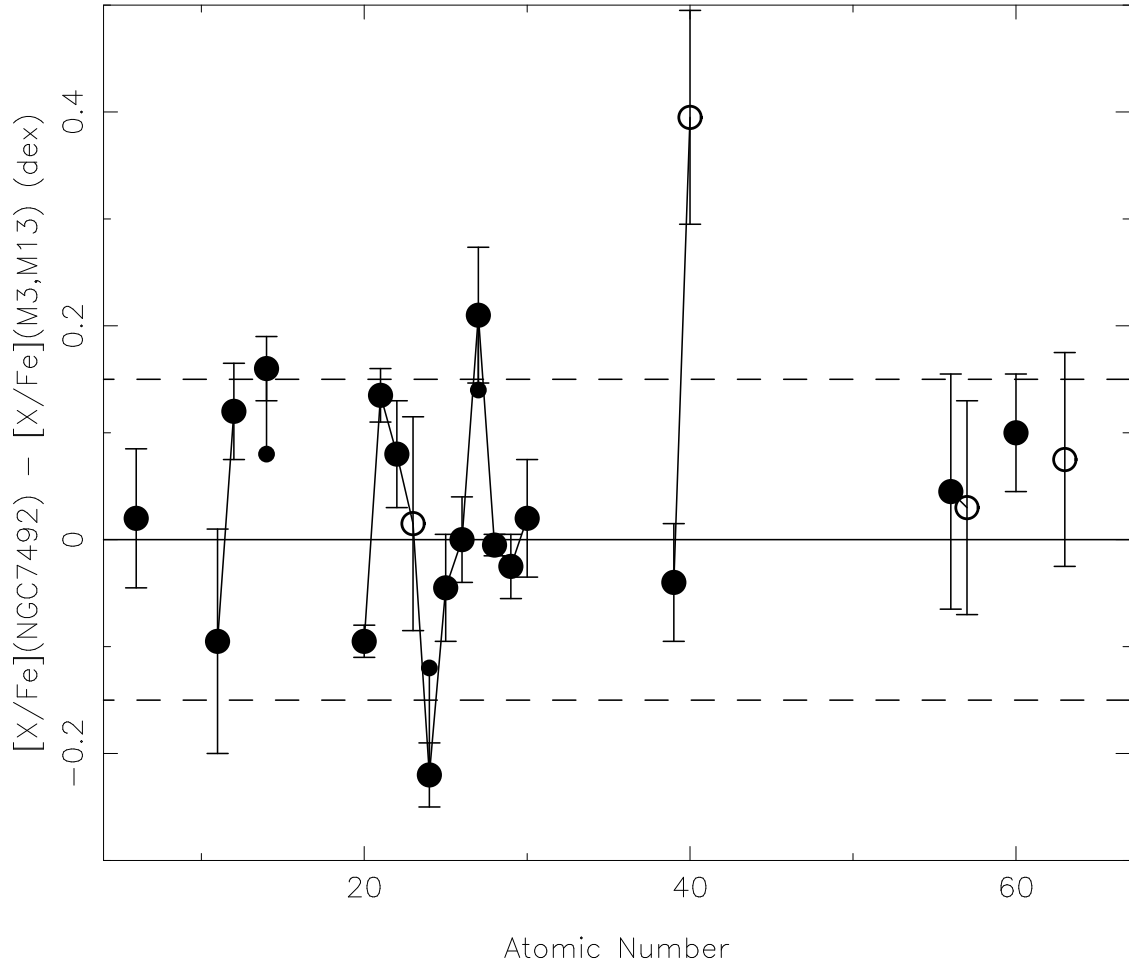
Fig. 10.— The abundance ratios [X/Fe] for NGC 7492, with the mean [X/Fe] for M3 and M13
subtracted, are shown as a function of atomic number. Open circles denote elements which have
been detected in only one star in the NGC 7492 HIRES sample. Lines connect the points where
consecutive atomic numbers have been detected. The dashed horizontal lines indicate the toler-
ance of ±0.15 dex about equality. Small filled circles indicate the results for Si, Cr and Co after
corrections for global trends in abundance ratio with metallicity have been applied.